

Effect of nanoparticles on the dielectric properties of polyimide

This article has been downloaded from IOPscience. Please scroll down to see the full text article.

2011 Smart Mater. Struct. 20 094001

(<http://iopscience.iop.org/0964-1726/20/9/094001>)

View [the table of contents for this issue](#), or go to the [journal homepage](#) for more

Download details:

IP Address: 131.84.11.215

The article was downloaded on 27/09/2011 at 15:26

Please note that [terms and conditions apply](#).

Report Documentation Page

Form Approved
OMB No. 0704-0188

Public reporting burden for the collection of information is estimated to average 1 hour per response, including the time for reviewing instructions, searching existing data sources, gathering and maintaining the data needed, and completing and reviewing the collection of information. Send comments regarding this burden estimate or any other aspect of this collection of information, including suggestions for reducing this burden, to Washington Headquarters Services, Directorate for Information Operations and Reports, 1215 Jefferson Davis Highway, Suite 1204, Arlington VA 22202-4302. Respondents should be aware that notwithstanding any other provision of law, no person shall be subject to a penalty for failing to comply with a collection of information if it does not display a currently valid OMB control number.

1. REPORT DATE JUL 2011	2. REPORT TYPE	3. DATES COVERED 00-00-2011 to 00-00-2011	
4. TITLE AND SUBTITLE Effect of nanoparticles on the dielectric properties of polyimide		5a. CONTRACT NUMBER	
		5b. GRANT NUMBER	
		5c. PROGRAM ELEMENT NUMBER	
6. AUTHOR(S)		5d. PROJECT NUMBER	
		5e. TASK NUMBER	
		5f. WORK UNIT NUMBER	
7. PERFORMING ORGANIZATION NAME(S) AND ADDRESS(ES) US Naval Academy, Physics Department, Annapolis, MD, 21402		8. PERFORMING ORGANIZATION REPORT NUMBER	
9. SPONSORING/MONITORING AGENCY NAME(S) AND ADDRESS(ES)		10. SPONSOR/MONITOR'S ACRONYM(S)	
		11. SPONSOR/MONITOR'S REPORT NUMBER(S)	
12. DISTRIBUTION/AVAILABILITY STATEMENT Approved for public release; distribution unlimited			
13. SUPPLEMENTARY NOTES			
14. ABSTRACT As part of a search for a better dielectric for use in high energy density capacitors, polyimide (PI) films containing a layered material, zirconium orthophosphate, $ZrO(H_2PO_4)_2 \cdot xH_2O$ (&#945;-ZrP), were fabricated. PI has the advantage that it can be used to very high temperatures. To characterize the materials, x-ray diffraction (XRD), differential scanning calorimetry (DSC) thermogravimetric analysis (TGA), and dielectric measurements (permittivity, loss and breakdown strength) were made. The permittivity and loss studies were also carried out on both neat PI films and &#945;-ZrP. The XRD, DSC and TGA results are consistent with amorphous composites. The effects of water or other impurities were observed in all three kinds of dielectric studies on all three types of material. For example, the relative permittivity of the composites decreased strongly when water was removed from the materials. Nonetheless, some increase in the relative permittivity of the dry nanocomposites was observed. Impurity or water-associated loss peaks were observed in all three types of material. The frequency and temperature dependences of the loss peaks made it possible to identify which were true relaxations. The effect of water is to decrease the dielectric strength of the composites. However, in both the wet and dry materials, the dielectric strength exhibits a maximum at a loading of about 5 wt% &#945;-ZrP.			
15. SUBJECT TERMS			
16. SECURITY CLASSIFICATION OF:			17. LIMITATION OF ABSTRACT
a. REPORT unclassified	b. ABSTRACT unclassified	c. THIS PAGE unclassified	Same as Report (SAR)
			18. NUMBER OF PAGES 10
			19a. NAME OF RESPONSIBLE PERSON

Effect of nanoparticles on the dielectric properties of polyimide

Naima Bestaoui-Spurr¹, C A Edmondson², M C Wintersgill²,
J J Fontanella² and Todd Adams¹

¹ Lynntech, Incorporated, 2501 Earl Rudder Frwy S, College Station, TX 77845, USA

² Physics Department, US Naval Academy, Annapolis, MD 21402, USA

E-mail: Naima.Bestaoui@Lynntech.com

Received 31 January 2011, in final form 7 July 2011

Published 30 August 2011

Online at stacks.iop.org/SMS/20/094001

Abstract

As part of a search for a better dielectric for use in high energy density capacitors, polyimide (PI) films containing a layered material, zirconium orthophosphate, $ZrO(H_2PO_4)_2 \cdot xH_2O$ (α -ZrP), were fabricated. PI has the advantage that it can be used to very high temperatures. To characterize the materials, x-ray diffraction (XRD), differential scanning calorimetry (DSC), thermogravimetric analysis (TGA), and dielectric measurements (permittivity, loss and breakdown strength) were made. The permittivity and loss studies were also carried out on both neat PI films and α -ZrP. The XRD, DSC and TGA results are consistent with amorphous composites. The effects of water or other impurities were observed in all three kinds of dielectric studies on all three types of material. For example, the relative permittivity of the composites decreased strongly when water was removed from the materials. Nonetheless, some increase in the relative permittivity of the dry nanocomposites was observed. Impurity or water-associated loss peaks were observed in all three types of material. The frequency and temperature dependences of the loss peaks made it possible to identify which were true relaxations. The effect of water is to decrease the dielectric strength of the composites. However, in both the wet and dry materials, the dielectric strength exhibits a maximum at a loading of about 5 wt% α -ZrP.

1. Introduction

With an ever increasing demand for higher energy density capacitors, there has been a renewed interest in developing new materials with improved dielectric properties. Further, it is highly desirable to find materials capable of operating at high temperatures. The equation that describes the energy density, μ , in a material is

$$\mu = \frac{1}{2}\kappa E^2 = \frac{1}{2}\epsilon_0\epsilon' E^2 \quad (1)$$

where ϵ_0 is the permittivity of free space, κ and ϵ' are the real part of the permittivity and the relative permittivity of the material, respectively, and E is the electric field. Two of the goals associated with materials design, then, are to maximize E and ϵ' . There is another electrical property, the dielectric loss, described either by the imaginary part of the relative permittivity, ϵ'' , or by $\tan \delta$, that must also be considered. As can be inferred from the name, this loss needs to be minimized at the operating frequencies and temperatures of the capacitor.

In many cases, the highest allowable value of $\tan \delta$ is of the order of 0.01. The maximum electric field that can exist in a material without breakdown is referred to as either the breakdown field or the dielectric strength. Because the energy density varies as the square of E , the dielectric strength is particularly important.

As has been pointed out in a review of recent work in the field [1], from about 2002 it was widely recognized that polymer/inorganic filler composites are promising materials for improved dielectric material and work on them began to accelerate. Because the book by Nelson provides both the rationale for the study of polymer nanocomposites or nanodielectrics and a summary of recent work [1], a detailed overview will not be given here. However, some important features of the field are as follows. Polymer nanodielectrics often combine the high value of relative permittivity of the inorganic nanofiller and the high breakdown strength, processability and flexibility of the polymer. In general, though, the high ϵ' of the filler does not have much effect on

the overall dielectric until very high loading concentrations [2]. The simple physical blend of an inorganic filler with a polymer seldom leads to a composite with enhanced dielectric properties. One problem that this approach often suffers from is excessive agglomeration of the filler due to the incompatibility with the polymer matrix. This usually causes cracking of thin films, thereby increasing the dielectric loss and reducing the electrical breakdown strength. Some help is obtained when the filler is nanosized, approaching the polymer chain conformation length. In that case, it acts 'cooperatively' with the host structure resulting in materials with enhanced dielectric, mechanical and thermal properties [3–5]. However, the best materials, by far, are made via suitable modification of the polymer, the surface of the nanoparticle, or both. This approach more often leads to aggregate-free composites and this technique forms the basis of the present work. Inherent in the case of nanoparticles is the large interface volume that exists in the region between the nanoparticles and the polymer. Improvements in properties such as dielectric breakdown or the mechanical properties of the nano-composites, leading to the ability to prepare thinner membranes are often attributed, at least in part, to the interface layer [6].

In the present work, polymer nanocomposites were made using polyimide (PI) and a layered material, zirconium orthophosphate, $\text{ZrO}(\text{H}_2\text{PO}_4)_2 \cdot x\text{H}_2\text{O}$ (α -ZrP), as the filler material. Two of the reasons why polyimide was chosen are that it is a high temperature material and it has a relatively high dielectric strength³. A layered material was chosen for the filler because layers have the potential to block charge flow and hence possibly make breakdown more difficult. In addition, α -ZrP has a medium high ϵ' of about 50 that varies very slightly up to 200 °C [7]. α -zirconium phosphate (α -ZrP) is a solid acid with Van der Waals bound layers of thickness 0.76 nm. The structure is similar to that of Montmorillonite clay. In α -ZrP the layers are formed by zirconium atoms connected via the oxygen atoms of the phosphate groups. Each phosphate contributes three of its oxygen atoms to the formation of these layers, leaving one OH group that is hydrogen bonded to a water molecule pointing into the interlayer space. Any two adjacent layers are displaced relative to one another so that cavities are formed between the layers. The free OH groups that point into the interlayer space form a staggered bilayer of hydroxyl groups [8]. There are no interlayer hydrogen bonds because the OH protons hydrogen-bond to the water, which in turn H-bonds to oxygens in the same layer.

To make α -ZrP compatible with polyimide and obtain a polymer nanocomposite, the α -ZrP surface was altered. Fortunately, the surface of α -ZrP can be easily modified by various charge-carrying ionic moieties that achieve polymerization and exfoliation of α -ZrP in various polymer systems [9–11]. In fact, published studies show that α -ZrP is capable of incorporating 2 mol of *n*-alkylamines with the formation of a bilayer in the interlayer space [12, 13]. This occurs either through hydrogen bonding or via an acid–base reaction, where the proton is transferred from the –POH group to the nitrogen. It is well known that even when as little as one amine is intercalated in α -ZrP, a bilayer is formed. In

³ DuPont™ Kapton®: technical information.

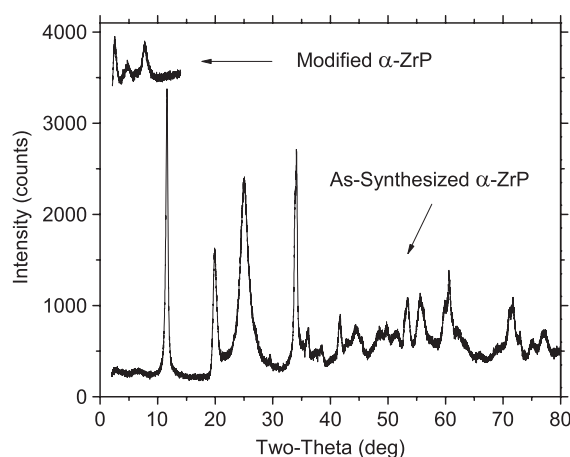


Figure 1. X-ray diffraction of as-synthesized and modified α -ZrP. The scales (counts) are the same for the two plots but the results for modified α -ZrP have been shifted upward for clarity.

this case presumably only every other –POH group interacts with an amine molecule. However, penetration does not occur but rather the angle at which the amine is inclined to the layers is smaller, decreasing the interlayer distance. The films were prepared by a solution casting process and it appears that the fabrication process resulted in a uniform distribution of the nanolayers with no agglomeration. A wide variety of techniques were used to characterize the films.

2. Experimental details

2.1. Sample preparation

α -ZrP was prepared by refluxing zirconyl chloride (30.64 g) in 3 M phosphoric acid (500 ml) for 24 h. The resulting powder was washed three times with deionized water, and then dried in an oven at 60 °C for 24 h. The resulting white material was ground, sieved, then surface modified in dimethylformamide (DMF) through an acid–base reaction. The modifier containing an amine group was dissolved in DMF and then added drop wise to a solution made of a suspension of α -ZrP in DMF, resulting in an almost transparent solution. The corresponding amount of PI needed to make a specific composition was then added and thoroughly mixed, then cast onto a glass support. The resulting films were heat treated then peeled out of the support after drying. Films containing various loadings of α -ZrP were prepared.

2.2. Characterization

2.2.1. X-ray diffraction. X-ray diffraction was used to assess the success of the α -ZrP synthesis, its surface modification and the formation of polymer nanocomposites. In the case of α -ZrP, the data give insight into interplanar spacings while the powder pattern of each compound was recorded on a Rigaku Miniflex x-ray diffractometer from 2° to 80° (in 2θ) with a step size of 0.04°/step and a scan speed of 1.2° min⁻¹. Typical results are shown in figures 1 and 2.

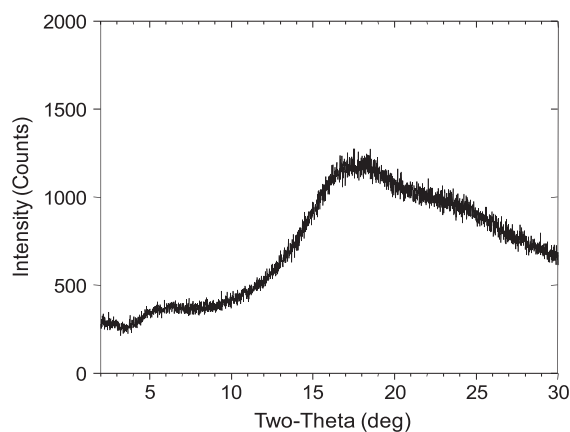


Figure 2. Typical polyimide/ α -ZrP nanocomposite x-ray diffraction pattern.

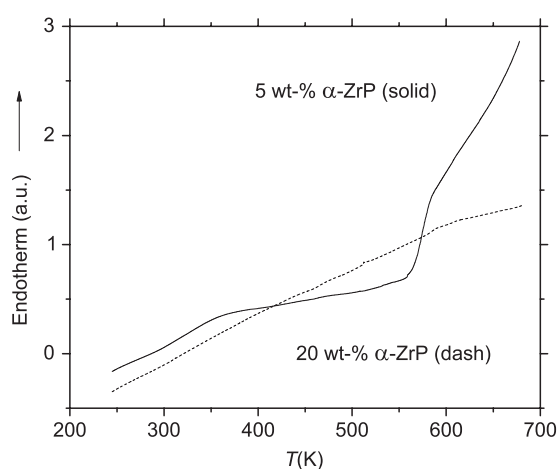


Figure 3. Differential scanning calorimetry results for PI containing 5 and 20 wt% α -ZrP. The data shown are the second heat for each material.

2.2.2. Thermal analyses. In order to further characterize the nanocomposite films containing surface modified α -ZrP, differential scanning calorimetry (DSC) and thermogravimetric analysis (TGA) were both carried out using a standard temperature ramp rate of 10 K min^{-1} . DSC gives insight into the crystallinity associated with the materials in that it is particularly sensitive to crystalline melting. In addition, DSC is capable of characterizing glass transitions. Typical results are shown in figure 3.

TGA is a direct measure of the weight loss of a material as it is heated and typical results are shown in figure 4. TGA is particularly useful for the materials studied in the present work because, as will be shown, water strongly affects the properties of PI- α -ZrP nanocomposites.

2.2.3. Dielectric permittivity. Because the goal is to develop better capacitor materials, the electrical properties of the nanocomposite films are important. Consequently, measurements leading to values of the relative permittivity, loss and dielectric breakdown were carried out. In order to carry out measurements of the relative permittivity and loss,

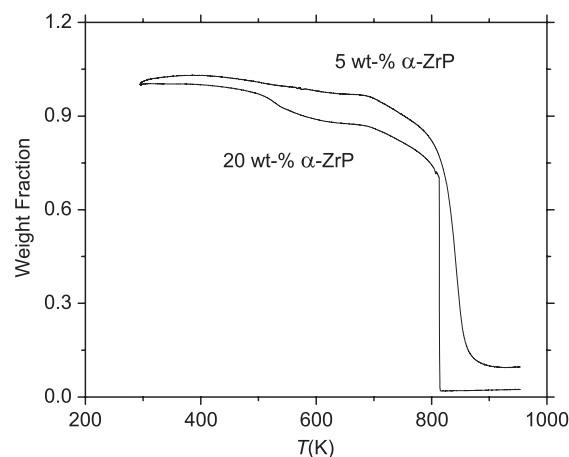


Figure 4. Thermogravimetric results for PI containing 5 and 20 wt% α -ZrP.

either aluminum was evaporated or gold was sputtered onto the surfaces of the nanocomposite films. Typical samples were $10 \mu\text{m}$ thick and 10–15 mm in diameter. Complex conductance measurements were carried out as discussed elsewhere [14]. The method, briefly stated, was to use a CGA-85 capacitance measuring assembly, which operates at 17 frequencies from 10 to 10^5 Hz. Measurements of the equivalent parallel conductance, G , and capacitance, C , were made. Two different systems were used to vary the temperature. Measurements were carried out in vacuum from 5.5 to 350 K in a Precision Cryogenics CT-14 dewar and the temperature was controlled using a LakeShore Cryotronics DR92 temperature controller. Other measurements were carried out at atmospheric pressure in flowing nitrogen gas using a Novocontrol sample holder and a Quatro temperature controller. That system operated at temperatures from 125 to 523 K.

The data were transformed to the complex relative permittivity as follows. First, geometrical measurements of the area, A , and thickness, d , of the samples were made and the real part of the relative permittivity (ϵ') at 1000 Hz was calculated at room temperature using the usual equation for a parallel plate capacitor:

$$C = \frac{\epsilon_0 \epsilon' A}{d}. \quad (2)$$

The values of ϵ' at the remaining temperatures and frequencies were calculated using the approximation that ϵ' scales as the capacitance, i.e. thermal expansion is ignored. Finally, the imaginary part of the relative permittivity (ϵ'') at all temperatures was calculated using

$$\epsilon'' = \epsilon' \frac{G}{\omega C} \quad (3)$$

where ω is the applied angular frequency. The loss is also sometimes characterized using $\tan \delta$ defined by

$$\tan \delta = \frac{\epsilon''}{\epsilon'}. \quad (4)$$

The data for the films are given in figures 5–11.

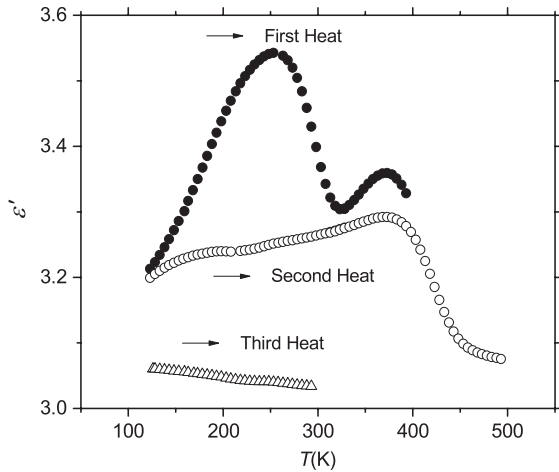


Figure 5. Real part of the relative permittivity versus temperature at 1000 Hz for a control PI (0 wt% α -ZrP).

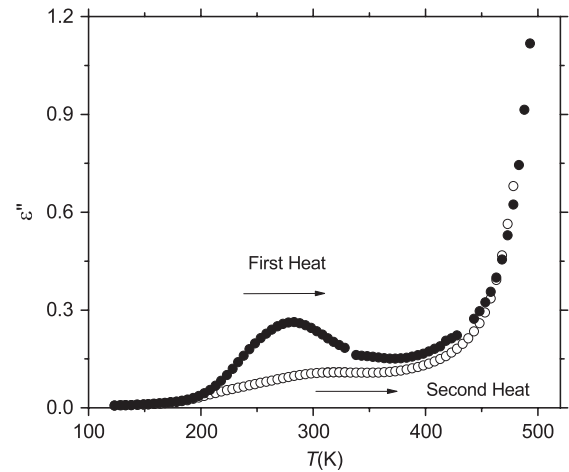


Figure 8. Imaginary part of the relative permittivity versus temperature at 1000 Hz for PI containing 20 wt% α -ZrP.

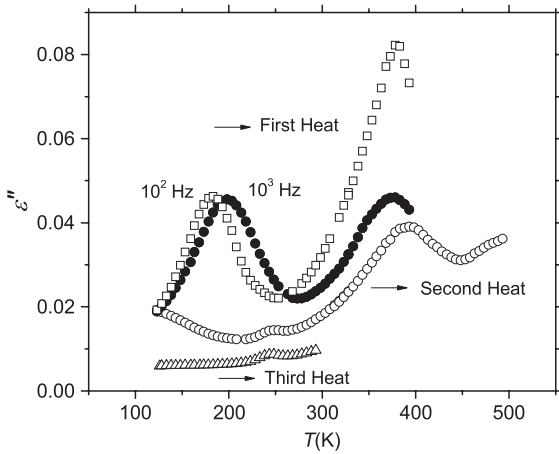


Figure 6. Imaginary part of the relative permittivity versus temperature for a control PI (0 wt% α -ZrP). For the first heat, both 10^2 Hz (open squares) and 10^3 Hz (closed circles) data are shown. The second and third heat data are for 1000 Hz only.

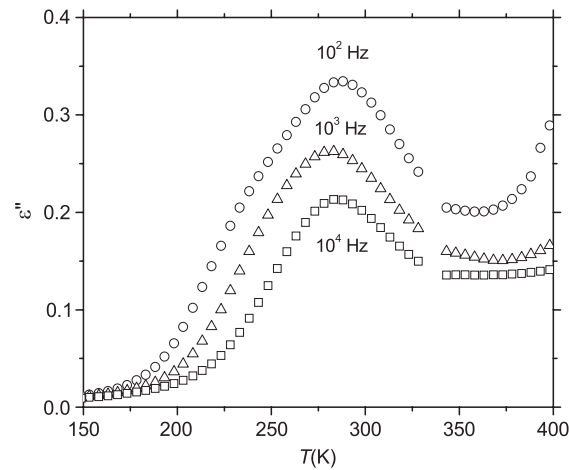


Figure 9. Imaginary part of the relative permittivity versus temperature at three frequencies for PI containing 20 wt% α -ZrP (the first heat of figure 8).

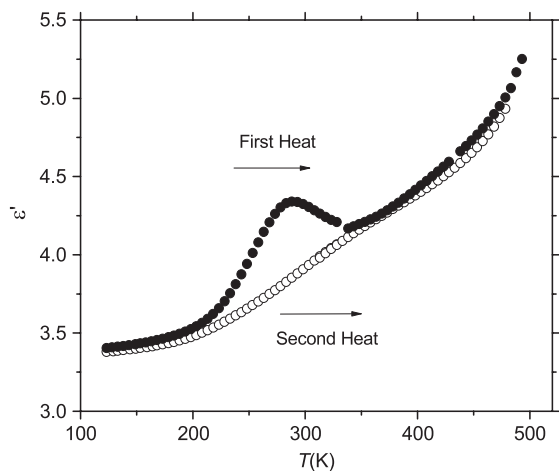


Figure 7. Real part of the relative permittivity versus temperature at 1000 Hz for PI containing 20 wt% α -ZrP.

For the permittivity measurements on the α -ZrP nanoparticles a different technique was used and is the same as given elsewhere for oxide nanoparticles [15]. Briefly, the nanopar-

ticles were placed in a cavity for the capacitance and conductance measurements. Because the geometry associated with the powders is unknown, the absolute relative permittivity of the nanoparticles themselves was not obtained. Rather, what is quoted is the effective relative permittivity of the cell containing the nanoparticles. In the present case, the real part of the permittivity of the cell at the lowest temperature was arbitrarily set equal to 3 and the calculations of the imaginary part were carried out using equation (3). The results for the real and imaginary parts of the effective relative permittivity during three heating cycles are shown in figures 12 and 13.

2.2.4. Dielectric breakdown. The DC dielectric strength was measured using a Hippotronics model HD140 Auto A AC/DC hipot tester. The sample was immersed in a Fluorinert FC-77 high dielectric strength fluid to suppress surface events that were not indicative of the bulk dielectric properties. The sample was placed on a polished conducting steel ground plane. The upper electrode was a 1 cm diameter tool steel

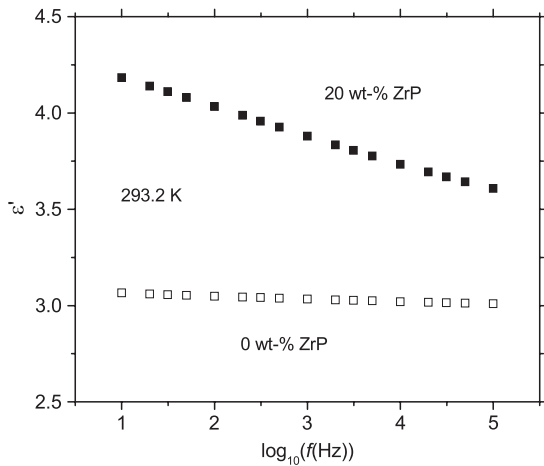


Figure 10. Real part of the relative permittivity versus frequency at about 293.2 K for PI and PI containing 20 wt% α -ZrP. Both samples had been heated to 493 K in nitrogen before measurement. The data correspond to those of the third heat in figure 5 and the second heat in figure 7.

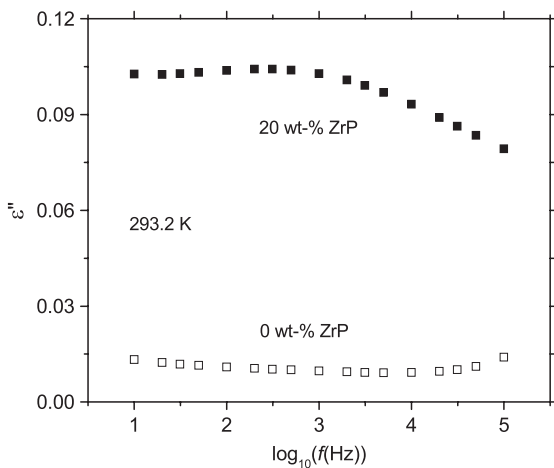


Figure 11. Imaginary part of the relative permittivity versus frequency at about 293.2 K for PI and PI containing 20 wt% α -ZrP. Both samples had been heated to 493 K in nitrogen before measurement. The data correspond to those of the third heat in figure 5 and the second heat in figure 7.

post approximately 75 mm in length. The weight of the post was used to establish a consistent contact pressure between the electrodes and the sample. The edge of the cylindrical electrode post was radiused in accordance with the ASTM D3755 test procedure in order to minimize the probability of edge breakdown during testing. The face of the electrode was polished to a mirror finish with 0.1 μm polishing compound to minimize the probability of a breakdown event being initiated by the surface texture of the electrode. A voltage ramp rate of 500 VDC s^{-1} was used throughout the test. The Hippotronics was set to trigger at a current of 1 mA for all tests.

The applied voltage, V , at breakdown was converted to an electric field using the measured sample thickness ($E = V/d$). The cumulative probability for failure was estimated using the median rank approximation. A Weibull two parameter

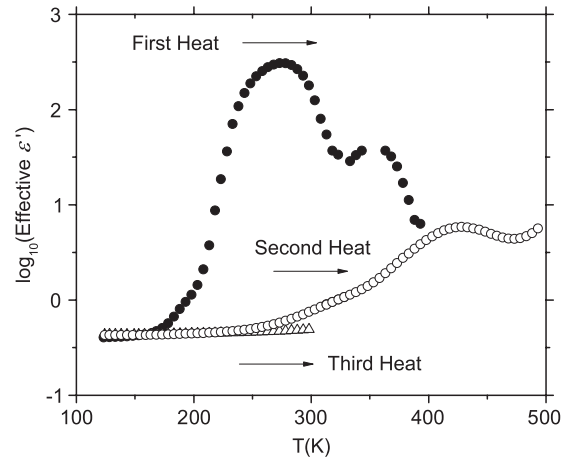


Figure 12. Logarithm of the effective real part of the relative permittivity versus temperature at 1000 Hz for α -ZrP nanoparticles placed in a cavity. The solid circles, open circles and triangles represent the first heat, second heat and third heat, respectively.

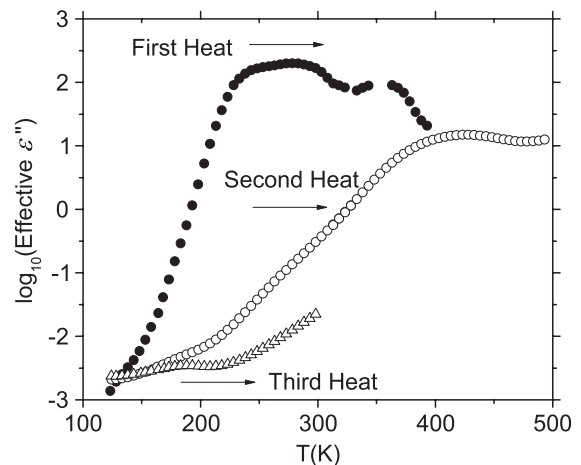


Figure 13. Logarithm of the effective imaginary part of the relative permittivity versus temperature at 1000 Hz for α -ZrP nanoparticles placed in a cavity. The solid circles, open circles and triangles represent the first heat, second heat and third heat, respectively.

probability distribution

$$P(E) = 1 - e^{-\left(\frac{E}{E_0}\right)^{\alpha_w}} \quad (5)$$

was fitted to the experimental data. $P(E)$ is the cumulative probability of failure for a given electric field, E . E_0 is the (characteristic) electric field with a 63.2% probability of failure and will be referred to throughout the paper as the dielectric strength. The exponent α_w is a shape parameter that is related to the spread in observed values.

The samples were initially tested after being exposed to normal room atmospheric conditions. However, the observed dielectric strengths were very low. Also, as will be described, permittivity and loss measurements showed changes with thermal annealing that were indicative of absorbed water related effects. Consequently, the dielectric strength was also measured after the samples had been annealed at 493 K under vacuum for 24 h and transferred directly to a glove box. (The

vacuum furnace was built into the glove box.) The glove box environment was maintained at or below 0.27 ppm water, while in the glove box the samples were immersed in Fluorinert FC-77, a hydrophobic liquid. The immersed samples were then removed from the glove box and re-tested for dielectric strength.

3. Results and discussion

3.1. α -ZrP

The x-ray powder pattern of α -ZrP (figure 1) as-synthesized consisted of broadened peaks that were all indexed as α -ZrP. No impurity peaks were found. The peak broadening indicated that the compound was not perfectly crystallized (because the acid used was dilute) and the interlayer spacing was approximately 0.76 nm. A scanning electron micrograph showed the formation of aggregates, which consisted of many irregular small particles. The size of the aggregated particles varied between 0.3 and 2 μ m.

After surface modification, the powder pattern (inset at the top of figure 1) was significantly different and was characteristic of a layered compound with only the 00 ℓ reflections observed. This is due to the severe preferred orientation exhibited by these materials. Also, upon surface modification, the interlayer spacing increases from 0.76 to 3.8 nm.

The powder patterns of the composite materials were representative of an amorphous compound in that no long range order was observed. Typical results are shown in figure 2. The broad maximum centered on about 20° in 2θ corresponds to polyimide.

3.2. Thermal analyses

Most of the materials showed a broad endothermic DSC feature starting at temperatures around 350 K. The data in figure 3 for the 5 wt% material are typical, though the feature is not prominent in the data for the 20 wt% sample. This feature was generally observed in the heating segments but not during cooling. Partly because of the onset temperature and partly because of the irreversibility, this feature is attributed to the loss of water from the samples. As will be shown, this is consistent with all of the other types of data for these materials. At higher temperatures, typically starting around 575 K, most of the samples showed some endothermic features on the heating segments. In some cases, the data exhibited characteristics similar to those of a glass transition. The data in figure 3 for the 5 wt% material are an example. However, many of the data did not exhibit characteristics of a glass transition and most of the results were not consistently reflected in the cooling segments. The origin of these features is not clear. Several possibilities include loss of residual modifier, DMF or tightly bound water. Similar results have been reported previously [16].

As can be seen in figure 4, the TGA data showed a loss in weight over most of the range of temperatures. Over the range from about 400 to 650 K, in the samples containing 5 wt% α -ZrP, there was a 6 wt% weight loss, but in the material

Table 1. The real part of the relative permittivity at 1000 Hz and room temperature for the polymer nanocomposite. The first column is the α -ZrP content in wt% and the second column is the real part of the relative permittivity for the as-prepared material. The third column contains ϵ' for a few dried materials. The uncertainty in ϵ' is ± 0.3 .

Wt% α -ZrP	ϵ' as-prepared	ϵ' dried
0	3.4	3.05
1	3.2	
5	4.5	
10	5.7	
20	8.9	3.9
20	9.3	

containing 20 wt% α -ZrP, the weight loss was double that. It is possible that the higher temperature TGA results (rapid drop above about 520 K) are associated with the higher temperature DSC data. Again, this may be attributable to residual modifier, DMF or tightly bound water. It is also consistent with a glass transition because rapid weight loss often happens above the glass transition temperature.

3.3. Permittivity

The real part of the relative permittivity at room temperature for several as-prepared materials is listed in table 1. The control samples (0 wt% α -ZrP) exhibited an average of about 3.4 and that is approximately equal to the value usually quoted for Kapton® [12]. The results in table 1 show that the real part of the relative permittivity for the as-prepared materials increases rapidly as α -ZrP content increases. However, as will be shown, all of these values depend strongly on the water content of the samples.

The first experiment that was carried out was to vary the temperature for the control samples. The first data run (first heat) was from about 125 to 400 K. The sample was then cooled again and data were taken from 125 to 500 K (second heat). The sample was cooled a third time and data were taken from 125 to 300 K (third heat). The results for the real part of the relative permittivity (ϵ') at 1000 Hz are shown in figure 5. It is clear that ϵ' is strongly affected by the thermal history of the sample. For example, after heating to 400 K, ϵ' decreases from a room temperature value of about 3.4 to about 3.25. After heating to 500 K, ϵ' decreases further to about 3.05. In order to get a clearer picture of the reason for the behavior, the imaginary part of the relative permittivity is shown in figure 6.

It is clear from figure 6 that during the first heat the as-prepared material exhibits a strong peak at 1000 Hz and about 200 K. (This is associated with the peak in ϵ' (figure 5) at about 250 K.) To show that this is a true relaxation, both 10^2 and 10^3 Hz data are shown. The behavior is 'normal' for a dipole in that the peak shifts to higher temperature as frequency increases and there is a slight decrease in the peak height indicative of $1/T$ Curie-type behavior. This feature is reminiscent of the water-associated relaxation that has been reported for polyetherimide [14]. In the case of polyetherimide, the water-associated relaxation at 1000 Hz occurs at a slightly higher temperature, 250 K, than the water

relaxation in polyimide for which it occurs at about 200 K. It is clear from a comparison of the first and second heat data that this relaxation disappears after heating the sample to 400 K. The removal of this relaxation in the case of polyimide accompanies the decrease in ϵ' from 3.4 to 3.25 described above. This relaxation and the associated increased ϵ' are attributed to loosely bound or physisorbed water.

The first heat data also show a peak at about 375 K. This is a non-relaxation associated peak caused by an impurity (for example, tightly bound or chemisorbed water) leaving the sample. The initial rise as temperature increases is caused by increasing mobility of the impurity and the subsequent decrease is attributed to irreversible loss of the impurity from the sample. The characteristic feature is that the peaks for both the 100 and 1000 Hz data occur at about the same temperature as opposed to the case for relaxations where the higher frequency peak occurs at a higher temperature as discussed previously for the lower temperature peak.

The second heat data show a peak at about 400 K. (There is also a very small feature at about 250 K in both the second and third heats. That will not be considered further in the present paper.) The 400 K peak is related to the 1000 Hz peak at about 375 K observed during the first heat. That the peak position shifts from the first heat to the second heat is another indication that this peak is not a true relaxation. The decrease in strength observed as temperature increases is attributable to a decreasing amount of an impurity in the sample as it is heated. The ϵ' data shown in figure 5 are also interesting in this regard. It is important to note that while heating the materials to 400 K only decreases the high temperature peak, the second heat data show that it appears to completely eliminate the 200 K relaxation/peak. This implies that two different types of water would be necessary to explain the origin of the two different peaks. Of course, either or both peaks may also be attributable to another impurity such as the solvent used in the casting process.

Data were not taken above 300 K during the third heat so the status of the 375/400 K peak after heating to 500 K is not known at the present time. However, the data suggest the possibility that it does not exist after heating to 500 K. Finally, the second heat data in figure 6 also indicate the presence of a 1000 Hz relaxation with a peak below 100 K. This relaxation disappears after heating the material to 500 K and accompanies the decrease in ϵ' from about 3.25 to 3.05 as described above.

Next, a study of the effect of thermal treatment on the room temperature value of ϵ' for the materials containing α -ZrP was carried out. The as-prepared 20 wt% sample that exhibited an ϵ' of 8.9 at room temperature was heated to about 500 K in vacuum then cooled slowly in vacuum. The capacitance was re-measured. Assuming that the change in capacitance is due to the change in ϵ' , a significant decrease in the ϵ' from 8.9 to 4.2 was found. (The dimensions of the samples were also measured before and after heat treatment. No change in dimensions was found.) However, the capacitance measurements were carried out in air and the values were increasing during the measurement. As an indication of the rate of change, the sample was left overnight in the laboratory and the next day ϵ' had increased to 6.4. The

sample continued to recover and after about a week ϵ' had increased to 7.0. These very large changes are attributed to the extra water uptake caused by the presence of the α -ZrP. Based on figure 5, a small contribution to the water uptake from polyimide itself is also expected.

This same 20 wt% sample was loaded into the variable temperature cell and the results for ϵ' and ϵ'' versus temperature are shown in figures 7 and 8, respectively, and the frequency variation is shown in figures 9–11. In general figure 7 shows that ϵ' increases as temperature increases and there is a peak at about 280 K in the ϵ' versus temperature on the first heat. Interestingly, as is also apparent from figure 7, the room temperature ϵ' at 1000 Hz was of the order of 4.2 even though the sample had previously recovered, exhibiting a higher value of ϵ' . That the value is lower is attributed to the equilibration/drying of the sample in flowing dry nitrogen before the temperature run. However, after heating to 490 K, the room temperature value was observed to be lower still, approximately 3.9. Also, there is no strong peak in the relative permittivity versus temperature. It is concluded that 3.9 is approximately equal to the value of the 1000 Hz ϵ' for dry PI containing 20 wt% of α -ZrP nanoparticles and this is significantly higher than the value of 3.05 found for dry PI.

Figure 8 shows the apparent loss peak associated with the peak in the real part of the relative permittivity versus temperature. Figure 9 shows this peak at three different frequencies. It is clear that this is not a true dielectric loss peak because the peak does not shift to higher temperatures as the frequencies increase. In fact, the 100 Hz peak is at a slightly higher temperature than the 1000 Hz peak. Also, the value of ϵ'' at all three frequencies begins to decrease at about the same temperature. Again, this behavior suggests that the peak occurs because of an impurity, probably water, leaving the sample as temperature increases. Further, it may be true that this peak, seen dielectrically at about 280 K, is associated with the DSC and TGA features that occur in the vicinity of 350 K. The significant difference in temperatures at which the effects of water loss are observed in the TGA and DSC results compared with the dielectric loss data is attributed to the difference in heating procedures. Both DSC and TGA are carried out at a constant heating rate of 10 K min⁻¹ whereas the dielectric measurements were made at a series of discrete temperatures after the sample had equilibrated for about 20 min at each temperature. However, one clarification is useful. In the case of the control PI (0 wt% α -ZrP) the low temperature peak (at about 200 K in figure 6) is a true relaxation and it is water-associated. It corresponds to the peak observed in polyetherimide [14] and remains observable so long as the sample is not placed in vacuum or heated above room temperature. This peak was not observed in any of the nanocomposite materials.

Figures 10 and 11 show the dispersion of ϵ' and ϵ'' after thermal treatment for both PI and PI containing 20 wt% of α -ZrP. The data for ϵ' in figure 10 show a larger variation with frequency for PI containing 20 wt% of α -ZrP than for PI. This is consistent with figure 11 where it is seen that the loss in the 20 wt% material is about an order of magnitude larger than for PI. The presence of the α -ZrP is presumed to be

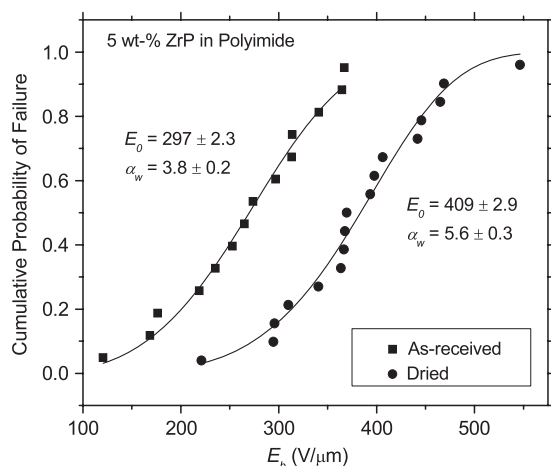


Figure 14. Cumulative probability of failure versus applied electric field for a sample containing 5 wt% α -ZrP.

the cause of the larger loss in PI containing 20 wt% of α -ZrP. However, whether the extra loss is associated with the polymer (e.g. defects introduced by the presence of the α -ZrP) or with the particles themselves is not known at the present time.

Finally, the dielectric properties of the nanoparticles themselves were studied using the technique described earlier. The results shown in figures 12 and 13 have a feature in common with those for the PI containing α -ZrP (the peak in ϵ'' at about 300 K) and are reminiscent of the higher temperature behavior exhibited by mesoporous silica and γ alumina [15]. There is an apparent peak (complex in the case of α -ZrP) at about 300 K in the effective imaginary part of the relative permittivity (ϵ''). Again, this is not true dielectric relaxation in that it is caused by water leaving the nanoparticles as temperature increases. The initial increase in either the real or imaginary part of the relative permittivity (leading edge of the apparent peak) is attributed to increasing mobility of protons or hydroxyl groups on the surfaces of the particles. The ultimate decrease is caused by the concentration of water decreasing as temperature increases. In the case of α -ZrP, however, there is also a higher temperature peak. This may be due to differently bound water.

3.4. Dielectric breakdown

Figure 14 is a plot of the cumulative probability of failure as a function of applied electric field for a sample containing 5 wt% α -ZrP. The characteristic field, E_0 , is used as a measure of the dielectric strength and, at room condition, is $297 \text{ V } \mu\text{m}^{-1}$ compared to the dried sample's value of $409 \text{ V } \mu\text{m}^{-1}$. The Weibull fit parameters for the remaining α -ZrP samples are listed in table 2 and the values of E_0 are plotted versus α -ZrP content in figure 15.

All samples showed improved dielectric strengths following the drying process. The average sample improved by approximately $150 \text{ V } \mu\text{m}^{-1}$. Figure 15 shows that a maximum in E_0 is found at approximately 5 wt% α -ZrP. While this concentration had the highest dielectric strength in both dried and as-prepared states, it is also the concentration

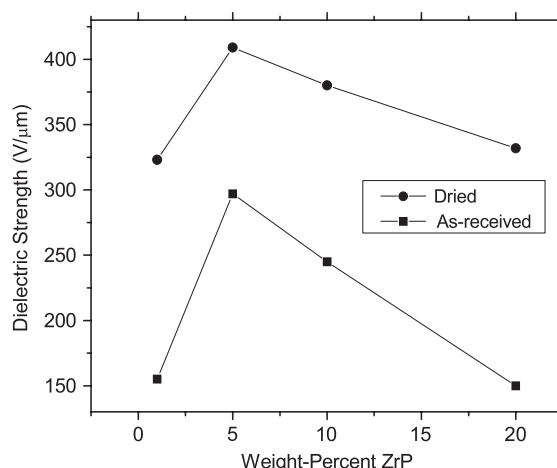


Figure 15. Dielectric strength for various amounts of α -ZrP in PI.

Table 2. Dielectric strength of polyimide containing α -ZrP nanoparticles. A significant increase in the dielectric strength is observed when the samples are dried.

Wt-% α -ZrP	As-prepared		Dried	
	E_0 ($\text{V } \mu\text{m}^{-1}$)	α_w	E_0 ($\text{V } \mu\text{m}^{-1}$)	α_w
1	155 ± 1.4	4.4 ± 0.3	315 ± 3.6	5.6 ± 0.7
5	297 ± 2.3	3.8 ± 0.2	409 ± 2.9	5.6 ± 0.3
10	247 ± 2.2	5.6 ± 0.4	371 ± 1.6	9.6 ± 0.7
20	150 ± 1.0	6.9 ± 0.5	329 ± 1.8	8.8 ± 0.7

with the least improvement upon drying. A maximum in the plot of dielectric strength versus nanoparticle concentration is not unusual. For example, Dou *et al* reported a maximum in the dielectric strength of barium titanate–polyvinylidene fluoride nanocomposites at a concentration of 7 vol% [17]. It is interesting to note that the maximum was observed for nanocomposites fabricated using surface modified barium titanate but was not observed when uncoated nanoparticles were used.

Finally, it is important to keep in mind that because the energy density (equation (1)) varies as the square of the electric field, the 38% improvement in the dielectric strength observed in the present work for the dried 5 wt% sample, for example, represents a 90% increase in the energy density.

4. Conclusions

As part of an ongoing effort to develop better capacitor materials, polymer nanocomposites were fabricated with varying amounts of α -ZrP in polyimide and the electrical properties were studied. The surface of α -ZrP was successfully modified to make it compatible with the polymer. Its incorporation at various loadings in polyimide resulted in polymer nanocomposites that were amorphous, as evidenced by x-ray, DSC and TGA studies. Several effects of moisture or other impurities were observed. The complex relative permittivity increased with increasing water content. The real part of the relative permittivity showed a strong increase with α -ZrP content. However, there was a large decrease in ϵ' for

α -ZrP when the samples were dried. Nonetheless, the value of ϵ' for the dry films increased somewhat with the loading. Next, peaks were observed in plots of the relative permittivity versus temperature. Most, but not all, of those were not true dielectric relaxations as they were caused by water or other impurities leaving the samples during the measurement procedure. Also, the dielectric strength was found to decrease with increasing water content. However, a maximum in the dielectric strength was found at 5 wt% loading of α -ZrP for both the as-prepared and the dried material.

Acknowledgments

This work was supported in part by the Office of Naval Research under contract No. N00014-08-0189. The authors would like to thank Mark Westgate for technical assistance.

References

- [1] Nelson J K (ed) 2010 *Dielectric Polymer Nanocomposites* (New York: Springer)
- [2] Calame J P 2008 *J. Appl. Phys.* **104** 114108
- [3] Lewis T J 1994 *IEEE Trans. Dielectr. Electr. Insul.* **1** 812–25
- [4] Imai T, Hirano Y, Hirai H, Kojima S and Shimizu T 2002 *IEEE ISEI* pp 379–83
- [5] Nelson J K, Fothergill J C, Dissado L A and Peasgood W 2002 *IEEE-CEIDP* pp 295–8
- [6] Roy M, Nelson J K, MacCrone R K, Schadler L S, Reed C W, Keefe R and Zenger W 2005 *IEEE Trans. Dielectr. Electr. Insul.* **12** 629–43
- [7] Costantino U 1982 *Inorganic Ion Exchange Materials* ed A Clearfield (Boca Raton, FL: CRC Press) chapter 3
- [8] Clearfield A and Smith G D 1969 *Inorg. Chem.* **8** 431–6
- [9] Troup J M and Clearfield A 1977 *Inorg. Chem.* **16** 3311–4
- [10] Bestaoui N, Spurr N and Clearfield A 2006 Intercalation of polyether amines into α -zirconium phosphate *J. Mater. Chem.* **8** 759–64
- [11] Sue H-J, Gam K T, Bestaoui N, Spurr N and Clearfield A 2004 *Chem. Mater.* **16** 242–9
- [12] Sue H-J, Gam K T, Bestaoui N, Clearfield A, Miyamoto M and Miyatake N 2004 *Acta Mater.* **52** 2239–50
- [13] Michel E and Weiss A 1965 *Z. Naturf.* **B20** 1307–8
- [14] Fontanella J J, Bendler J T, Schuele D E, Edmondson C A and Lomax J F 2007 *J. Non-Cryst. Solids* **353** 4528–32
- [15] Fontanella J J, Wintersgill M C, Edmondson C A and Lomax J F 2009 *J. Phys. D: Appl. Phys.* **42** 042003
- [16] Kim C H, Yim H S and Jeon C 1998 *Solid State Commun.* **106** 535–40
- [17] Dou X, Liu X, Zhang Y, Feng H, Chen J-F and Du S 2009 *Appl. Phys. Lett.* **95** 132904